Marine and Petroleum Geology 86 (2017) 1406–1416

Contents lists available at ScienceDirect

Marine and Petroleum Geology

journal homepage: www.elsevier.com/locate/marpetgeo

Research paper

Controls of hydrocarbon generation on the development of expulsion fractures in organic-rich shale: Based on the Paleogene Shahejie Formation in the Jiyang Depression, Bohai Bay Basin, East China

Cunfei Ma [a, b, *], Derek Elsworth [b], Chunmei Dong [a, c, d], Chengyan Lin [a, c, d], Guoqiang Luan [a], Bingyi Chen [a], Xiaocen Liu [a], Jawad Munawar Muhammad [a], Aleem Zahid Muhammad [a], Zhengchun Shen [e], Fuchun Tian [f]

[a] School of Geosciences, China University of Petroleum (East China), Qingdao 266580, China
[b] Department of Energy and Mineral Engineering, College of Earth and Mineral Sciences, The Pennsylvania State University, University Park, PA 16802, USA
[c] Reservoir Geology Key Laboratory of Shandong Province (East China), Qingdao 266580, China
[d] Research Laboratory of China University of Petroleum (East China), Key Laboratory of Oil and Gas Reservoir, Qingdao 266580, China
[e] Research Institute of Exploration and Development, Shengli Oilfield Company, SINOPEC, Dongying 257015, China
[f] Petroleum Engineering Research Institute of Dagang Oilfield, Tianjin 300280, China

ARTICLE INFO

Article history:
Received 20 September 2016
Received in revised form
24 July 2017
Accepted 28 July 2017
Available online 29 July 2017

Keywords:
Shale oil
Expulsion fractures
Characteristics
Thermal simulation experiments
Influencing factors
Development model
Jiyang Depression

ABSTRACT

The development of expulsion fractures in organic-rich shale is closely related to hydrocarbon generation and expulsion from kerogen. Organic-rich shales from the upper part of the fourth member and the lower part of the third member of the Paleogene Shahejie Formation in the Jiyang Depression, Bohai Bay Basin, East China, are used as an example. Based on thin sections, SEM and thermal simulation experiments, the characteristics of hydrocarbon generation and the conditions supporting the development of expulsion fractures were explored. The key factors influencing these fractures include the presence of kerogens, their distribution along laminae and around particle boundaries, their exposure to heat and the build-up in pressure due to confinement by low permeability. The development of excess pore fluid pressures and intrinsic low rock fracture strength are the main influencing factors. Pressurization by rapid generation of hydrocarbon provides impetus for fracture initiation and cause bitumen to migrate quickly. The shale laminae results in distinctly lower fracture strength laminae-parallel than laminae-normal and this directs the formation of new fractures in the direction of weakness. When pore fluid pressure increases, maximum and minimum principal effective stresses decrease by different proportions with a larger reduction in the maximum principal effective stress. This increases the deviatoric stress and reduces the mean stress, thus driving the rock towards failure. Moreover, the tabular shape of the kerogen aids the generation of hydrocarbon and the initiation of expulsion fractures from the tip and edge. The resulting fractures extend along the laminae when the tensile strength is lower in the vertical direction than in the horizontal direction. Particle contact boundaries are weak and allow fractures to expand around particles and to curve as the stress/strength regime changes. When pore fluid pressure fields at different fracture tips overlap, fractures will propagate and interconnect, forming a network. This paper could provide us more detailed understanding of the forming processes of expulsion fractures and better comprehension about hydrocarbon expulsion (primary migration) in source rocks.

© 2017 Published by Elsevier Ltd.

1. Introduction

Shale oil is an important unconventional hydrocarbon resource. The successful exploitation of shale oil in the Marcellus shale in the United States (Kargbo et al., 2010) has triggered research into understanding the formation of such deposits - as the key to identifying sweet spots for their recovery. Fractures are the main

* Corresponding author. School of Geosciences, China University of Petroleum (East China), Qingdao 266580, China.
E-mail address: mcf-625@163.com (C. Ma).

http://dx.doi.org/10.1016/j.marpetgeo.2017.07.035
0264-8172/© 2017 Published by Elsevier Ltd.

pathways for the primary migration of hydrocarbon (Fan et al., 2010; Jin and Johnson, 2008; Katz, 2012; Katz et al., 2017; Lash and Engelder, 2005, 2009; Ozkaya, 1984). Gale et al. (2014) provides a systematic summary of the types of fractures in shale, which include fractures at a high angle to bedding, bed-parallel fractures, early compacted fractures, and fractures associated with concretions. Laminae-parallel fractures that commonly develop in organic-rich shale - identified as expulsion fractures in this article - are intrinsically related to hydrocarbon generation from kerogen and its subsequent expulsion (Ding et al., 2012, 2013; Fan et al., 2010; Lash and Engelder, 2005, 2009; Ozkaya, 1988; Rodrigues et al., 2009; Vernik, 1994). This process was observed in thermal simulation experiments (Figueroa Pilz et al., 2017; Korost et al., 2012; Panahi et al., 2013). Korost et al. (2012) discussed the reaction of matter of high organic content with a low maturation grade clayey carbonate rock sample that is heated in a nitrogen atmosphere. Alteration in pore space structures is monitored in this way, which is very helpful for the successful prediction of nontraditional reservoir zones. Panahi et al. (2013) and Figueroa Pilz et al. (2017) discussed the nucleation and growth of microcracks that were imaged at the scale of the experiment. X-ray computed tomography was performed using synchrotron beam lines, making it possible to acquire images at resolutions of a few microns with short scanning times. Al Duhailan et al. (2013, 2016), Al Duhailan and Sonnenberg (2014) studiedy the characteristics and genesis of expulsion fractures in detail. On the basis of this previous research, we use organic-rich shale from the Paleogene Shahejie Formation in the Jiyang Depression, Bohai Bay Basin, East China, as a type-example to explore the processes involved in the evolution of expulsion fractures. We conducted thermal simulation experiments and observed the characteristics of expulsion fractures by SEM. Then, the discharge rate of fluid and expansion rate of sample were calculated, and the controlling factors and formation mechanisms were analyzed. Finally, we summarized the key processes involved in the development of expulsion fractures.

2. Overview of the study area

The Jiyang Depression with abundant lacustrine shale oil resources is a potential area for shale oil, and some oil wells have begun production. The Jiyang Depression is a first-order tectonic unit of the Bohai Bay Basin, East China, which is bounded to the west by the Tan-Lu Fault, to the south by the Chengning Uplift and to the north by the Luxi Uplift. The depression has a maximum length of 240 km from east to west, a maximum width of 130 km from south to north and a total area of 26000 km^2. It is a Mesozoic-Cenozoic fault-depressed basin that developed contemporaneously with the North China Craton. The Jiyang Depression features a tectonic pattern with salients and sags. There are four negative secondary tectonic units, namely, the Dongying, Huimin, Zhanhua and Chezhen Sags. A series of positive secondary tectonic units include Gudao, Yihezhuang, Chenjiazhuang, Wudi, Binxian and Kendong-Qingtuozi Salients. The Jiyang Depression has undergone three stages of tectonic evolution: a Mesozoic fault-depression stage, a Paleogene fault-depression stage and a Neogene depression stage. More importantly for this study, several sets of deep lake, organic-rich shales accumulated duringin the Paleogene fault-depression stage. The upper part of the fourth member and the lower part of the third member of the Shahejie Formation are thick and massive, with plenty of retarded oil (Katz et al., 2017). These are the main source rocks and major strata for shale oil exploration in East China. The organic-rich shale samples were collected from the Dongying Sag (FY 1 well, LY 1 well, NY 1 well) and the Zhanhua Sag (L69 well), as shown in Fig. 1.

3. Characteristics of expulsion fractures

Expulsion fractures are widely developed in the organic-rich shale of the upper part of the fourth member and the lower part of the third member of the Shahejie Formation in the Jiyang Depression. The fractures are closely related to kerogen genesis, and cracks develop through the middle, edge, or tip of kerogen molecules (Fig. 2a–c). Some fractures are connected with collophanite and microfossils (Dorozhkin, 2009) related to the biogenic origin (Fig. 2d–f). The crack width is from several micrometers to dozens of micrometers, and the length is from several micrometers to several centimeters. The wall of the fractures is uneven and bypasses particles, and most of the fractures are filled with bitumen (Fig. 2g–h, l, n). Fractures generated from two kerogens become closer and form a line or a rhomboic ring (Fig. 2i–j). However, fractures generated from several kerogens connect to form lines or arrange en echelon (Fig. 2k–l) and have extension or tension-shear characteristics. Most fractures extend horizontally and parallel to the direction of laminae (Fig. 2m–o), but some become curved at the end and turn towards one other (Fig. 2n). Some fractures extending horizontally are connected with each other through longitudinal fractures (Fig. 2o). If expulsion fractures develop abundantly in shale, a fracture network with a layered framework could be formed by end-to-end connections, turning connections and vertical connections (Fig. 2p).

4. Thermal simulation experiments on organic-rich shale

4.1. Samples and experimental facilities

Experimental samples were collected from the lower part of the third member of the Shahejie Formation encountered in the L69 well in the Zhanhua Sag. The lithology is grayish-brown oil shale with type I kerogen and an index of hydrocarbon generation, which belongs to high-quality source rock category with low-maturity organic matter (Table 1).

The thermal experiment was carried out by the School of Geosciences, China University of Petroleum (East China). The experimental facilities include an autoclave, a temperature control system and a pressure control system. In particular, the autoclave is made of hastelloy alloy with a maximum volume of 1000 ml, maximum tolerable temperature of 350 °C and maximum tolerable pressure of 50 MPa. The temperature control system is composed of a thermocouple, a temperature sensor and an AI-518P artificial intelligent temperature controller, which can control the heating process precisely. The pressure control system is composed of pressure sensor and GBS-STA100 gas-supercharging system.

4.2. Experimental scheme

Before the experiment, the fresh shale sample was cut perpendicular to lamina into 4 groups of regular lumpy samples; each group contained 6 experimental samples. Then, the mass and height of each sample were measured using a balance and a spiral micrometer. The thermal simulation experiment adopted the method of adding distilled water (Kobchenko et al., 2011; Lewan, 1997; Lewan and Roy, 2011), in the amount of 200 mL. In the experiment, we set four groups of different experimental temperatures and pressures. The initial temperature was 25 °C with experimental temperatures of 150 °C, 200 °C, 250 °C and 300 °C, and corresponding pressures of 15 MPa, 20 MPa, 25 MPa and 30 Mpa. These temperature and pressure conditions correspond to the formation pressure at depths of 1500 m, 2000 m, 2500 m and 3000 m underground, respectively. During the heating process,the temperature was set to increase at a constant rate and then remain

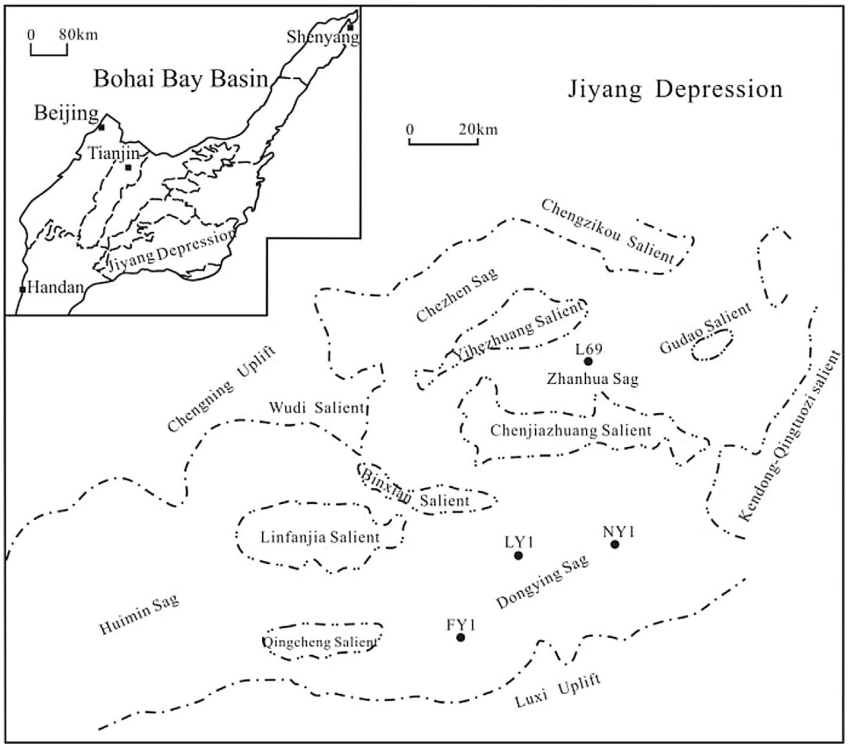

Fig. 1. Location of the study area.

constant (Dong et al., 2015), the heating stage lasted 4 h, and the steady-state stage lasted 48 h (Table 2).

4.3. Experimental results

After the experiment, samples were flushed with chloroform to remove the residual fluid including hydrocarbon and pore water, then they were put into a fume hood for air drying. After the samples were dried, the mass and height of every sample were measured again (Table 3). Because the sample generated and discharged fluid, which resulted in mass loss during the experiment, the mass loss rate, which can serve as the discharge rate, was calculated based on the mass variation of the sample before and after the experiment by Equation (1). The sample thermally expanded and fractured during the experiment, which led to a height increase, so the height increase rate, which can be regarded as expansion rate, can be calculated according to the height variation of the sample before and after the experiment by Equation (2).

$$D = (M_{pre} - M_{post})/M_{pre} \times 1000‰ \quad (1)$$

$$E = (H_{post} - H_{pre})/H_{pre} \times 100\% \quad (2)$$

In the equation, D refers to fluid's discharge rate, ‰; M_{pre} refers to the sample's mass before the experiment, g; M_{post} refers to sample's mass after the experiment, g; E refers to sample's expansion rate, %; H_{post} refers to the sample's height after the experiment, mm; H_{pre} refers to sample's height before the experiment, mm.

After the experiment, the samples were observed with a stereomicroscope and an environment scanning electron microscope (ESEM). It was observed that a large amount of expulsion fractures developed in the samples, which have similar characteristics to samples obtained from oil wells. Groups of fractures extend in a parallel relationship and distribute en echelon (Fig. 3a–c), with some fractures becoming curved at the end (Fig. 3a). The fractures usually initiate or expand along the tip or edge of kerogen molecules (Fig. 3d–f), and are filled with bitumen (Fig. 3g–h). Single fractures extend along the boundary between clay-rich laminae and carbonate-rich laminae (Fig. 3i), bypassing rigid felsic and carbonate minerals (Fig. 3j and k). The ends of the two fractures become curved or bifurcated (Fig. 3l–n) during facture growth (Fig. 3m and n), and finally, they connect with each other (Fig. 3o).

From the experiments, we find that as the temperature and pressure increase, the development and extent of expulsion fractures increase gradually. Before the experiment, in the original sample, kerogens were dispersed without fractures (Fig. 4a). At 150 °C, fractures started to form with small crack openings and short horizontal extensions that were isolated (Fig. 4b). At 200 °C, with kerogen as the core, additional fractures developed, and the crack openings and extension distance increased (Fig. 4c). At 250 °C, the ends of different fractures started to connect with each other (Fig. 4d). At 300 °C, the amount, extension distance and connectivity of fractures kept increasing (Fig. 4e and f).

5. Discussion

5.1. Factors influencing the formation of expulsion factures

5.1.1. Pore fluid pressure

In the experiment, hydrocarbons are generated and fractures form when the shale is put under increased temperature and pressure (Meng et al., 2010). For both samples, the expansion rate, which is related to fracture formation, and the fluid discharge rate,

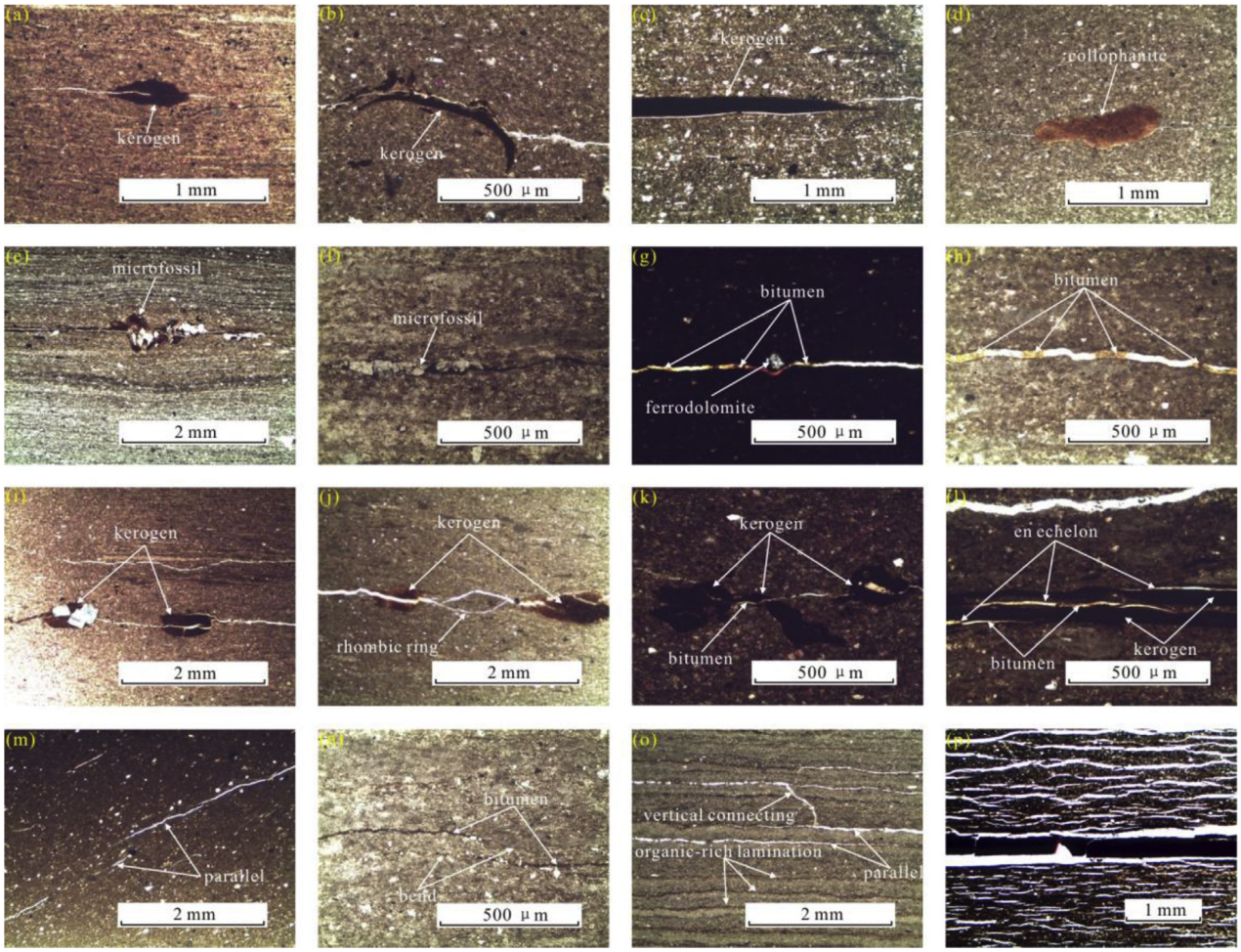

Fig. 2. Characteristics of the expulsion fracture in practical shale samples. (a) Fracture passing through the middle of the kerogen along the long axis direction; (b) fracture passing through the edge of the kerogen; (c) fracture cracking at the tip and extending along the edge of the kerogen; (d) fracture passing through the edge and tip of the collophanite; (e) fracture passing through the middle of the microfossil; (f) fracture passing through the tip and edge of the microfossil; (g) fracture bypassing the ferrodolomite and filled with bitumen; (h) fracture filled with bitumen; (i) fracture connecting two kerogens; (j) two fractures getting close and forming a rhomboic ring; (k) fracture connecting three kerogens; (l) fractures arranging in en echelon; (m) fractures distributing parallel; (n) two fractures bending to each other; (o) longitudinal fracture connecting horizontal fractures; (p) fracture networks with layered framework.

Table 1
Sample information.

Basic information		Kerogen maceral		Hydrocarbon generation index	
		Sapropelinite	97.3%	S1	0.55 mg/g
Well	L69 well	Exinite	0.3%	S2	14.06 mg/g
Depth	3053.10 m	Vitrinite	2.3%	Tmax	430 °C
Strata	the lower part of the third member	Inertinite	0.1%	TOC	4.37%
Lithology	grayish-brown oil shale	Kerogen type	I	Ro	0.6%

Table 2
The scheme of thermal simulation experiments.

Sample group number	Sample number	Experiment temperature/°C	Pressure/MPa	Amount of water/ml
I	I1~I6	150	15	200
II	II1~II6	200	20	200
III	III1~III6	250	25	200
IV	IV1~IV6	300	30	200

Notes: in the experiments, the initial temperature is 25/°C, the heating-up time is 4 h, and the thermostatic time is 48 h.

Table 3
Calculation on fluid's discharge rate and sample's expansion rate after the experiment.

Sample's group number	Sample's number	Mass before experiment/g	Mass after experiment/g	Fluid's discharge rate/‰	Height before experiment/mm	Height after experiment/mm	Sample's expansion rate/%
I	I1	1.62	1.61	6.2	9.225	9.300	0.8
	I2	2.43	2.42	4.1	7.303	7.343	0.5
	I3	3.48	3.46	5.7	8.212	8.265	0.6
	I4	4.84	4.83	2.1	11.887	11.967	0.7
	I5	15.37	15.34	1.9	16.560	16.612	0.3
	I6	10.79	10.76	2.8	17.441	17.480	0.2
II	II1	1.61	1.60	6.2	9.122	9.142	0.2
	II2	1.64	1.62	12.2	8.222	8.522	3.6
	II3	3.86	3.83	7.8	9.041	9.170	1.4
	II4	5.11	5.08	5.9	12.340	12.690	2.8
	II5	12.75	12.68	5.5	20.050	20.620	2.8
	II6	18.71	18.66	2.7	20.160	20.284	0.6
III	III1	1.10	1.09	9.1	6.660	6.900	3.6
	III2	1.26	1.24	15.9	7.230	7.270	0.6
	III3	2.65	2.62	11.3	7.930	8.150	2.8
	III4	3.03	2.98	16.5	7.222	7.650	5.9
	III5	9.03	8.96	7.8	14.292	14.870	4.0
	III6	9.09	9.01	8.8	9.422	9.748	3.5
IV	IV1	1.32	1.28	30.3	6.760	7.211	6.7
	IV2	2.01	1.97	19.9	13.006	13.618	4.7
	IV3	3.25	3.16	27.7	9.664	10.210	5.6
	IV4	3.33	3.27	18.0	12.100	12.754	5.4
	IV5	6.30	6.19	17.5	12.010	12.610	5.0
	IV6	9.40	9.28	12.8	12.300	12.916	5.0

which is related to hydrocarbon generation, increase exponentially as the temperature rises (Fig. 5a), and the two rates have a linear relationship (Fig. 5b). The direct relationship between these rates of change indicates that expulsion facture formation is closely related to hydrocarbon generation. The pressure increase by pyrogenic hydrocarbon generation is the main dynamic source for fluid overpressure inside the shale (Guo et al., 2011). The distribution of expulsion fractures matches the over-pressure position in the strata (Ma et al., 2016). Therefore, it can be concluded that pore fluid pressure by pyrogenic hydrocarbon generation from kerogen is one of the main factors for expulsion facture formation. Under a certain pressure field, pore fluid pressure can change the stress state of the rock matrix until it reaches the fracture strength of the rock and natural fluid pressure fractures form (Engelder and Lacazette, 1990).

Expulsion factures form when the pore fluid pressure builds to reach the rock's fracture strength. The speed of hydrocarbon generation greatly affects the increase in pore fluid pressure (Bredehoeft et al., 1994). Because shale has small pore-throats and low permeability, it is hard for fluid to discharge. Therefore, the amount and speed of hydrocarbon generation from kerogen are the main factors influencing pore fluid pressure accumulation. If the amount of hydrocarbon generation is constant, the faster the hydrocarbon generation speed is, the more advantageous the hydrocarbon accumulation is for pore fluid production. Generally, a rock's fracture strength is greater than the displacement pressure. If the speed of hydrocarbon generation is so slow that the amount is not adequate, and the force of hydrocarbon expulsion remains less than the displacement pressure, then the hydrocarbon will be trapped in pores and the pore fluid pressure will not reach the rock's fracture strength (Fig. 6A-a, Fig. 7a). If the speed of hydrocarbon generation is moderate, which results in a driving force of hydrocarbon expulsion greater than the displacement pressure but less than rock's fracture strength, then the hydrocarbon will flow until the amount of seepage and the amount of hydrocarbon generation become balanced. In this case, the pore fluid pressure will not accumulate to reach the rock's fracture strength, so no fracturing will occur (Fig. 6A-b, Fig. 7b). If the speed of hydrocarbon generation is high, and the amount of hydrocarbon generation is greater than the seepage amount, then the hydrocarbon will accumulate constantly and pore fluid pressure will continue increasing until it reaches the rock's fracture strength and generates fractures (Fig. 6A-c, Fig. 7c), which cause bitumen to migrate quickly. When shale is extremely tight and laminae develop abundantly or when the brittleness of the rock is great, fracture strength is less than displacement pressure, so pore fluid pressure can reach rock's fracture strength quickly, and expulsion fractures can form more easily (Fig. 6B-b and 6B-c).

5.1.2. Rock's fracture strength

Fractures form when the driving force reaches the rock's fracture strength, such as tensile strength and shearing strength. Shale contains fine particles and high clay mineral content with orientations that produce weak surfaces such as laminae (Aadnoy et al., 2009; Gallant et al., 2007). It is determined that the mechanical properties of shale have strong anisotropy, which can be illustrated by the fact that fracture strength in the direction perpendicular to laminae is greater than that parallel to laminae (Chenevert and Gatlin, 1965; Cheng et al., 2013; Mighani et al., 2016; Sayers, 2013; Schmidt, 1977; Sondergeld and Rai, 2011; Sone and Zoback, 2013a, 2013b; Waters et al., 2011). If the pore fluid pressure increases to reach the rock's fracture strength in the laminae-parallel direction, maleic fractures will form.

The rock's fabric is the key factor in determining the rock's fracture strength. Shale is composed of complicated components, including organic matter, clay minerals, felsic minerals and carbonate minerals. Organic matter is the material required for the pressure increase from hydrocarbon generation and is also one of necessary factors for expulsion fracture formation. Under the same pressure and temperature conditions, when shale contains higher organic matter content, more hydrocarbon is generated and pore fluid overpressure is more easily reached, making it better for

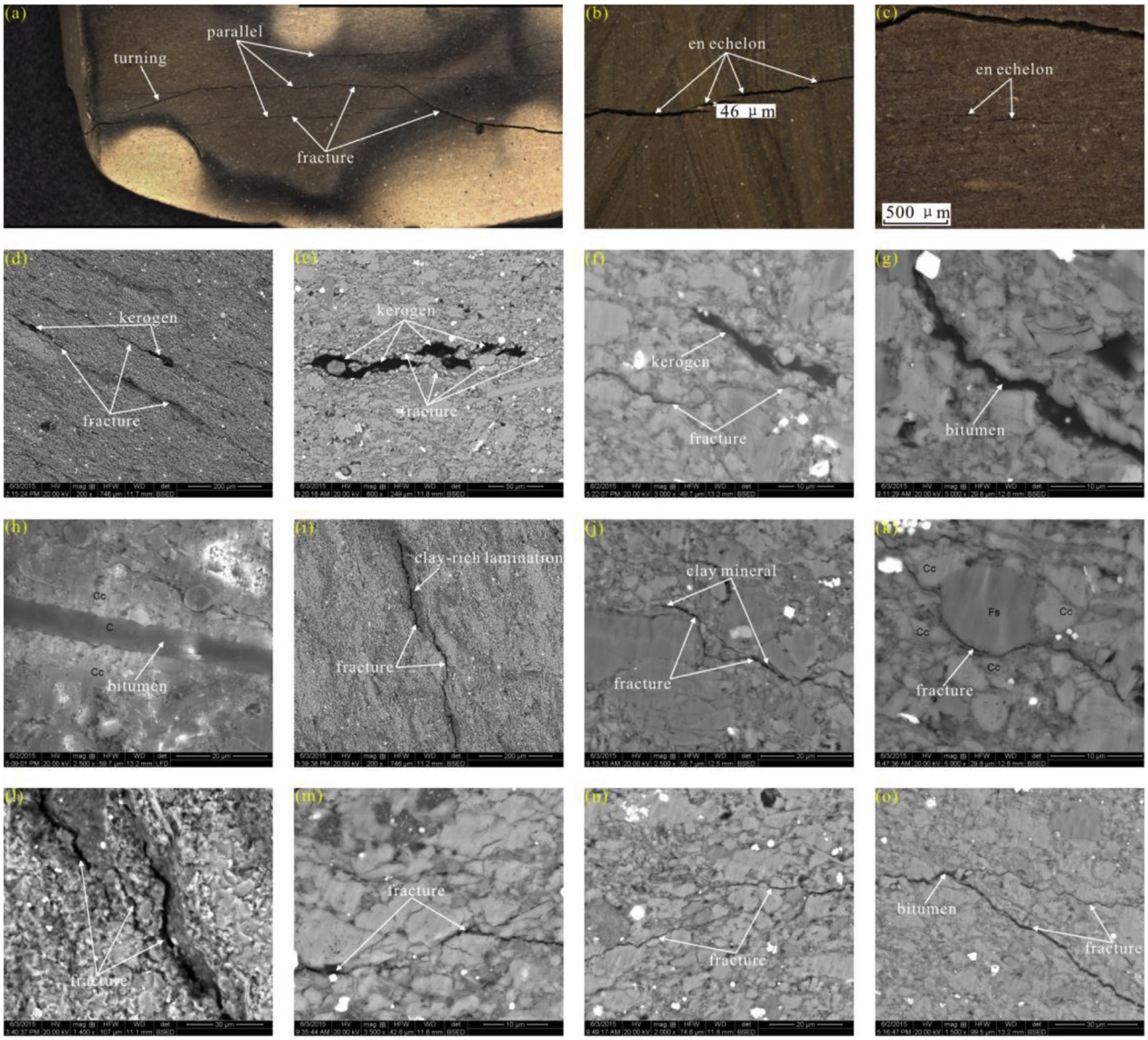

Fig. 3. Characteristics of expulsion fractures in samples after the experiment. (a) Fractures extending parallel or partially bending; (b),(c) fractures distributing in en echelon; (d) fractures with the core of kerogen; (e) fracture cracking from the edge and tip of kerogen; (f) fracture expanding near the kerogen; (g),(h) fracture filled with bitumen; (i) fracture extending along the boundary of lamina; (j),(k) fracture bypassing the mineral particles and extending along the contact boundary; (l) fractures bending and branching; (m),(n) the ends of two fractures bending and approaching each other; (o) two fractures intersecting.

expulsion fractures to form. There are three distribution patterns of organic matter and inorganic minerals in shale: scattered, semi-continuous and continuous (Fig. 8). Generally, it has the characteristics of directional and maleic distribution, thus making expulsion fractures extend parallel to laminae (Přikryl, 2001). During the heating process, the coefficient of thermal expansion is different in different parts of the sample, which leads to different deformation degrees and causes thermal stress at the edge of different minerals. Therefore, the contact boundary between organic matter and inorganic minerals or between inorganic minerals is mechanically weak (Feng and Zhao, 2015), and expulsion fractures will extend easily along the edge of particles. Therefore, the organic matter offers both the driving force and the crack initiation point for expulsion fractures. The directional distribution of the rock's components and their contact boundaries provide favorable conditions for the maleic expansion of fractures.

5.2. The mechanism of expulsion fracture cracking and expansion

When rock is buried at a certain stage, it becomes a porous elastic medium under diagenesis. The pore fluid pressure could change the local stress state of rock by producing an elastic response from the rock matrix, which influences the way fractures are generated. The influence on the stress state of the rock matrix by the pore fluid pressure can be expressed as Equation (3) (Engelder and Fischer, 1994; Goulty, 2003; Hillis, 2001; Yassir and Bell, 1994). When the vertical main stress remains stable, the horizontal main stress will increase as the pore fluid pressure increases

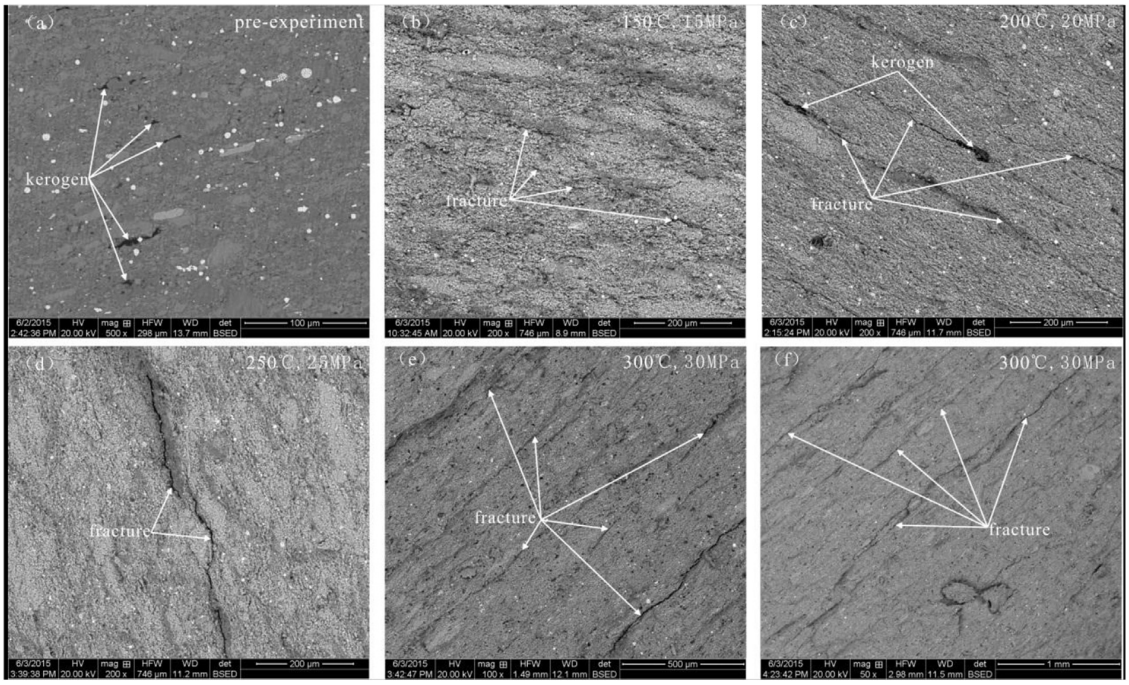

Fig. 4. Variation characteristics of the expulsion fracture along with the increase in temperature and pressure in samples after the experiment.

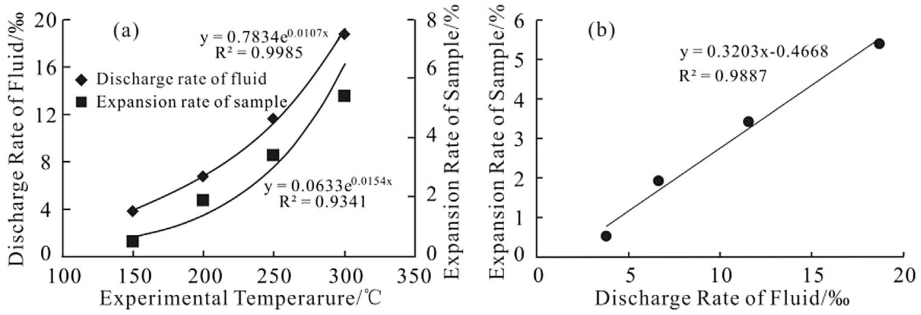

Fig. 5. The relationship among the sample's expansion rate, the fluid's discharge rate and the experimental temperature.

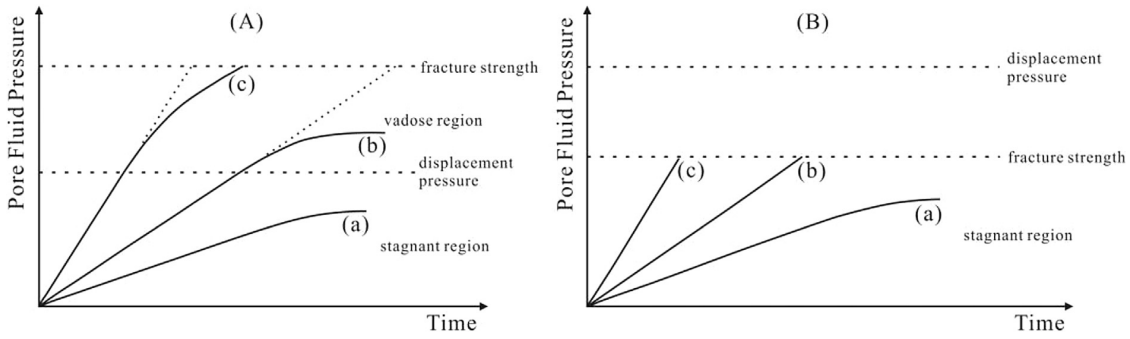

Fig. 6. The schematic diagram of the relationship between the rate of hydrocarbon generation and the formation of the expulsion fracture.

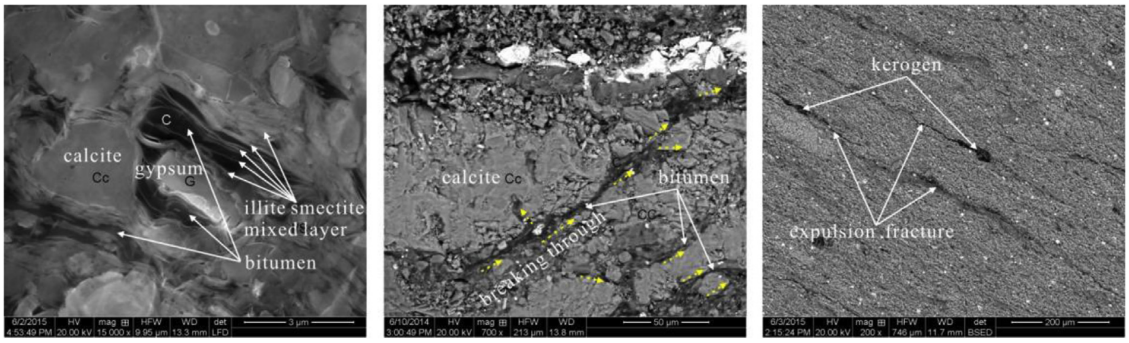

Fig. 7. The movement modes of bitumen. (a) bitumen retained in intercrystalline pores between clay flakes, (b) bitumen breaking through intercry - stalline pores between calcite crystals, (c) formation of expulsion fractures with a kerogen core.

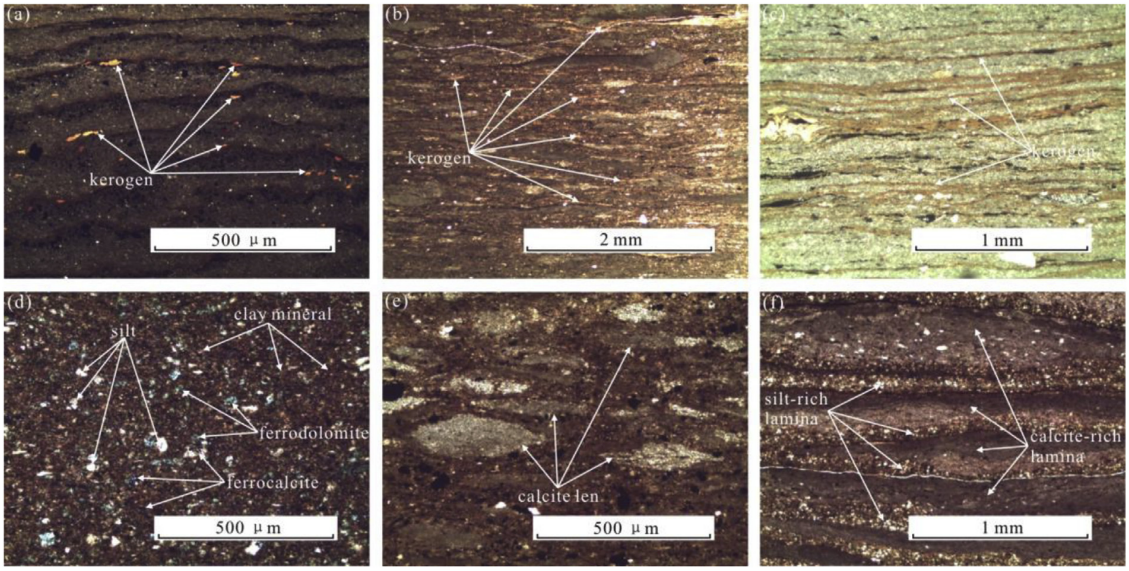

Fig. 8. Distribution patterns of organic matter and inorganic minerals in the shale.

because the Poisson's ratio is generally less than one.

$$S_h = \frac{\nu}{1-\nu}(S_v - \alpha P_p) + \alpha P_p \quad (3)$$

In the equation, S_h refers to horizontal main stress, S_v refers to vertical main stress, ν refers to Poisson's ratio, P_p refers to the pore fluid pressure, and α refers to the Biot coefficient.

When the overall stress can remain stable by deforming the rock's margin, the increase in pore fluid pressure will make the Mohr's circle move towards the left, and then Mohr's circle becomes tangent to the Mohr's envelope line, generating shearing fracture (Fig. 9). However, in the formation condition, because the degree of horizontal and vertical deformation in the rock is different, when the pore fluid pressure increases, the decrease in the extent of the horizontal main stress is lower than that of the vertical main stress. The difference between the maximum and minimum main stresses decreases, and the rock cracks horizontally and horizontal extension fractures form (Cobbold and Rodrigues, 2007; Cobbold et al., 2013; Luo et al., 2015).

Hydrocarbon generation from kerogen is a process in which the molecular weight decreases and the molecular number and overall volume increase. When kerogen is buried and enters the oil-generation window, the phase transition of organic matter will lead to a volume increase. Because of the small pores and the extremely low permeability of shale, the hydrocarbon cannot be expulsed in a timely manner, which makes the pore fluid pressure around kerogen increase dramatically. Meanwhile, under compaction, the tabular morphology of kerogen will make stress gather at the tip, which is of vital importance for forming horizontal fractures (Ozkaya, 1988). To study the relationship between kerogen morphology and the cracking conditions for maleic fractures, Ozkaya (1988) built an isotropy model for a hydrocarbon source according to a linear elastic condition. The model treats kerogen as a tabular particle and accounts for different kerogen morphologies by using a specific value K, which is a ratio between the horizontal length and vertical length of the kerogen. The permeability of the matrix around kerogen is considered to be zero. The Equation (4) (Ozkaya, 1988) reflects the relationship between kerogen's morphology and initial cracking of the expulsion fractures. According to Equation (4), the more tabular the kerogen morphology is, the greater the specific value will be and the lower the rock's tensile strength will be, allowing expulsion

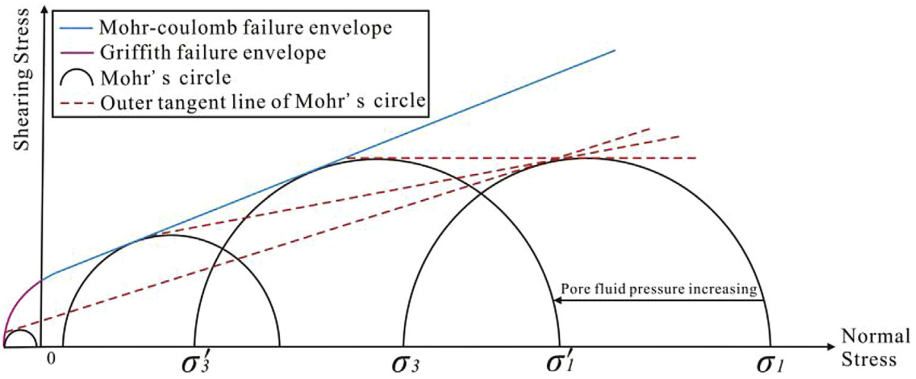

Fig. 9. The schematic diagram of the influence of pore fluid pressure on rock failure.

fractures to form more easily.

$$\Delta P_p > \frac{S_v(2-R)+T}{2K-1} \tag{4}$$

In the equation, ΔP_p refers to the pore fluid pressure caused by hydrocarbon generation of kerogen, S_v refers to the vertical main stress, R refers to the specific value between the horizontal main stress and the vertical main stress, T refers to the tensile strength, and K refers to the specific value between the horizontal length and vertical length of kerogen.

Laminae are well developed in organic-rich shale. Different laminae are composed of different components, so the cohesion between laminae is weak. Even in the same laminae, the clay minerals, felsic minerals and carbonate minerals are directionally distributed, which makes shale have anisotropic mechanical properties and makes the vertical tensile strength lower than the horizontal one (Schmidt, 1977). As a result, it is easier for the fractures to extend along laminae, in a direction with a lower tensile strength after the initial cracking at the tip of kerogen. During the process of fracture expansion, the ability to resist the vertical stress decreases as the pore fluid pressure decreases, which causes the crack opening to decrease. Meanwhile, the fractures extend and bypass particles because of low fracture toughness (Ovid'Ko, 2007). If the direction of the stress intensity factor changes at the end of the fractures, then the fracture orientation will change (Erdogan and Sih, 1963; Plank and Kuhn, 1999; Rice, 1968). During the process of fracture extension, if the pore fluid pressure fields overlap to influence each other, then two fractures generated from different kerogens become curved at the end and connect together vertically (Misra et al., 2009; Potluri et al., 2005).

5.3. The development model for expulsion fractures

The tabular kerogen generates hydrocarbon quickly under temperature and pressure with an increase in volume (Fig. 10a and b). Because of the small pore throats and the low permeability of shale, the hydrocarbon cannot be expulsed effectively. As a result, the pore fluid pressure increases inside and around the kerogen (Fig. 10c), thus causing stress to accumulate at the tip and edge of kerogen until it reaches the rock's fracture strength. Fractures initiate at the tip or edge of kerogen and are filled with hydrocarbon, forming expulsion fractures (Fig. 10c). The expulsion fractures extend along laminae as the crack opening decreases (Fig. 10c).

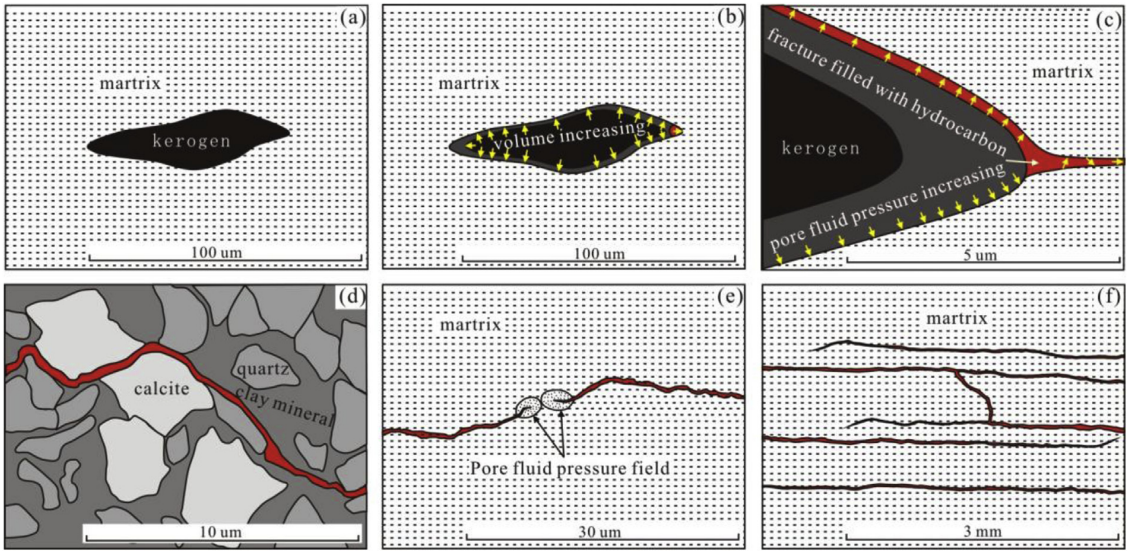

Fig. 10. The development pattern of the expulsion fracture.

During the extending process, fractures preferentially extend in pathways with lower fracture strength, such as edge of particles, boundary of laminae or pre-fractures (Fig. 10d). If the pore fluid pressure fields overlap, different expulsion fractures become curved at the end and get closer to each other and connect to form a fracture network (Fig. 10e and f).

6. Conclusions

(1) Expulsion fractures related to the increase in pore fluid pressure caused by hydrocarbon generation are commonly developed in organic-rich shale. The fractures take the kerogen as the initial cracking point and extend along laminae. Then the fractures expand along the edge of the particles and finally become curved at the end and connect with each other to form a fracture network.

(2) Thermal simulation experiments with high temperature and high pressure and with water added were conducted on organic-rich shale samples with low-maturity organic matter. The experiments verify that expulsion fractures develop well in laboratory samples and their characteristics are the same as in real world samples. The degree of development of expulsion fractures increases with the increase in experimental temperature and pressure.

(3) The pore fluid pressure and the fracture strength are the main factors influencing the formation of expulsion fractures. The faster the speed of hydrocarbon generation is, the more favorably the pore fluid pressure accumulates until it reaches the rock's fracture strength. The lower the rock's fracture strength is, the more easily the expulsion fracture forms. The directional distribution of organic matter and inorganic minerals produces a situation where rock's fracture strength parallel to the direction of laminae is lower than that perpendicular to laminae. The mechanical properties of the contact boundary between particles are weak and directionally distribute, which provides the conditions favoring the fractures' maleic extension and expansion by bypassing the particles.

(4) The increase in pore fluid pressure by hydrocarbon generation from kerogen leads to a decrease in the maximum and minimum main stresses to different extents. Moreover, the decrease in the maximum main stress is more obvious, Mohr's circle moves towards the left, and its radius decreases. Finally, the pressure reaches the rock's fracture strength and the rock cracks at the tip or edge of the kerogen. Because the laminae are well developed, the directional structure is obvious, and the anisotropy of mechanical properties is strong in shale. The vertical tensile strength is lower than the horizontal one, which results the expulsion fractures extending along the laminae direction. If the direction of the stress intensity factor changes or the pore fluid pressure fields overlap at the end of fractures, then the fractures will become curved and connect with each other. The detailed forming processes of expulsion fractures provides us better comprehension about hydrocarbon expulsion (primary migration) in source rocks.

Acknowledgements

This work was funded by China Scholarship Council (Grant No. 201506450031) and National Science and Technology Major Project, P.R. China (Grant No. 2011ZX05009-003, 2017ZX05009-001). We thank Professor Qiang Jin from China University of Petroleum (East China) for his constructive suggestions on the design of thermal simulation experiments. We thank Professor Terry Engelder and Professor Michael Arthur from the Pennsylvania State University for their beneficial discussion on the origin of expulsion fractures in shale.

References

Aadnoy, B., Hareland, G., Kustamsi, A., De, T., Hayes, J., 2009. Borehole failure related to bedding plane. In: Proceedings of the ARMA Conference, Asheville, North Carolina, June 28th-July 1.

Al Duhailan, M., Sonnenberg, S.A., Meckel, L.D., Meckel, L.D., 2013. Insights on hydrocarbon-generation microfracturing in organic-rich shales. In: Paper SPE 1515553 Presented at the 2013 Unconventional Resources Technology Conference, Denver, Colorado, USA, 12–14 August.

Al Duhailan, M., Sonnenberg, S., 2014. Impact of petroleum-expulsion fractures on productivity of the Bakken shales: A geological interpretation of pressure transient behaviors. Unconventional Resources Technology Conference, Denver, Colorado, USA, 25–27 August.

Al Duhailan, M., Boudjatit, M., Yeh, N. S., Kurison, I. L. C., Alvarez, A. R., Ghamdi, Y., Shehri, S., 2016. Integrated analysis of abnormal pressures in source rocks: theory and implications for Jurassic unconventional resource exploration in Saudi Arabia. Unconventional Resources Technology Conference, San Antonio, Texas, USA, 1–3 August.

Bredehoeft, J.D., Wesley, J.B., Fouch, T.D., 1994. Simulations of the origin of fluid pressure, fracture generation, and the movement of fluids in the Uinta Basin, Utah. AAPG Bull. 78, 1729–1747.

Chenevert, M.E., Gatlin, C., 1965. Mechanical anisotropies of laminated sedimentary rocks. SPE J. 5, 67–77.

Cheng, Q., Sondergeld, C., Rai, C., 2013. Experimental study of rock strength anisotropy and elastic modulus anisotropy. Seg. Tech. Program Expand. Abstr. 362–367.

Cobbold, P.R., Rodrigues, N., 2007. Seepage forces, important factors in the formation of horizontal hydraulic fractures and bedding-parallel fibrous veins ('beef' and 'cone-in-cone'). Geofluids 7, 313–322.

Cobbold, P.R., Zanella, A., Rodrigues, N., Løseth, H., 2013. Bedding-parallel fibrous veins (beef and cone-in-cone): worldwide occurrence and possible significance in terms of fluid overpressure, hydrocarbon generation and mineralization. Mar. Petroleum Geol. 43, 1–20.

Ding, W., Li, C., Xu, C., Jiu, K., Zeng, W., Wu, L., 2012. Fracture development in shale and its relation to gas accumulation. Geosci. Front. 3, 97–105.

Ding, W., Zhu, D., Cai, J., Gong, M., Chen, F., 2013. Analysis of the developmental characteristics and major regulating factors of fractures in marine-continental transitional shale gas reservoirs: a case study of the Carboniferous-Permian strata in the southeastern Ordos Basin, central China. Mar. Petroleum Geol. 45, 121–133.

Dong, C.M., Ma, C.F., Luan, G.Q., Lin, C.Y., Zhang, X.G., Ren, L.H., 2015. Pyrolysis simulation experiment and diagenesis evolution pattern of shale. Acta Sedimentol. Sin. 33, 1053–1061 (in Chinese with English abstract).

Dorozhkin, S.V., 2009. Calcium orthophosphates in nature, biology and medicine. Materials 2, 399–498.

Engelder, T., Fischer, M.P., 1994. Influence of poroelastic behavior on the magnitude of minimum horizontal stress, Sh in overpressured parts of sedimentary basins. Geology 22, 949–952.

Engelder, T., Lacazette, A., 1990. Natural hydraulic fracturing. In: Barton, C., Stephansson, O. (Eds.), Rock Joints. Balkema, Rotterdam, pp. 35–43.

Erdogan, F., Sih, G.C., 1963. On the crack extension in plates under plane loading and transverse shear. J. Basic Eng. 85, 519–525.

Fan, Z., Jin, Z., Johnson, S.E., 2010. Subcritical propagation of an oil-filled penny-shaped crack during kerogen-oil conversion. Geophys. J. Int. 182, 1141–1147.

Feng, Z., Zhao, Y., 2015. Pyrolytic cracking in coal: Meso-characteristics of pore and fissure evolution observed by micro-CT. J. China Coal Soc. 40, 103–108 (in Chinese with English abstract).

Figueroa Pilz, F., Dowey, P.J., Fauchille, A.L., Courtois, L., Bay, B., Ma, L., Lee, P.D., 2017. Synchrotron tomographic quantification of strain and fracture during simulated thermal maturation of an organic-rich shale, UK Kimmeridge Clay. J. Geophys. Res. Solid Earth 122, 1–12.

Gale, J.F., Laubach, S.E., Olson, J.E., Eichhubl, P., Fall, A., 2014. Natural fractures in shale: a review and new observations. AAPG Bull. 98, 2165–2216.

Gallant, C., Zhang, J., Wolfe, C.A., Freeman, J., Al-Bazali, T.M., Reese, M., 2007. Wellbore stability considerations for drilling high-angle wells through finely laminated shale: a case study from Terra Nova. In: Proceedings of the SPE Annual Technical Conference, Anaheim, 20–22 November.

Goulty, N.R., 2003. Reservoir stress path during depletion of Norwegian chalk oilfields. Pet. Geosci. 9, 233–241.

Guo, X., He, S., Song, G., Wang, X.J., Wang, B.J., Na, L.I., 2011. Evidences of overpressure caused by oil generation in Dongying depression. Earth Science-Journal China Univ. Geosciences 36, 1085–1094 (in Chinese with English abstract).

Hillis, R.R., 2001. Coupled changes in pore pressure and stress in oil fields and sedimentary basins. Pet. Geosci. 7, 419–425.

Jin, Z., Johnson, S.E., 2008. Primary oil migration through buoyancy-driven multiple fracture propagation: oil velocity and flux. Geophys. Res. Lett. 35, L09303.

Kargbo, D.M., Wilhelm, R.G., Campbell, D.J., 2010. Natural gas plays in the Marcellus shale: challenges and potential opportunities. Environ. Sci. Technol. 44,

5679–5684.
Katz, B.J., 2012. Hydrocarbon migration: what we know, what we don't know and why it is important. Houst. Geol. Soc. Bull. 55 (2), 15–17.
Katz, B.J., Arango, I., Frasse, F., 2017. Expulsion and migration associated with unconventional petroleum systems. Houst. Geol. Soc. Bull. 59, 23–25.
Kobchenko, M., Panahi, H., Renard, F., Dysthe, D.K., Malthe-Sørenssen, A., Mazzini, A., 2011. 4D imaging of fracturing in organic-rich shales during heating. J. Geophys. Res. Solid Earth 116 (B12).
Korost, D.V., Nadezhkin, D.V., Akhmanov, G.G., 2012. Pore space in source rock during the generation of hydrocarbons. Mosc. Univ. Geol. Bull. 67, 240–246.
Lash, G.G., Engelder, T., 2005. An analysis of horizontal microcracking during catagenesis: example from the Catskill delta complex. AAPG Bull. 89, 1433–1449.
Lash, G.G., Engelder, T., 2009. Tracking the burial and tectonic history of Devonian shale of the Appalachian Basin by analysis of joint intersection style. Geol. Soc. Am. Bull. 121, 265–277.
Lewan, M.D., 1997. Experiments on the role of water in petroleum formation. Geochimica Cosmochimica Acta 61, 3691–3723.
Lewan, M.D., Roy, S., 2011. Role of water in hydrocarbon generation from Type-I kerogen in Mahogany oil shale of the Green River Formation. Org. Geochem. 42, 31–41.
Luo, Y., Zhao, Y.C., Chen, H.H., Hui, S.U., 2015. Fracture characteristics under the coupling effect of tectonic stress and fluid pressure: a case study of the fractured shale oil reservoir in Liutun subsag, Dongpu Sag, Bohai Bay Basin, Eastern China. Petroleum Explor. Dev. 42, 177–185.
Ma, C.F., Dong, C.M., Luan, G.Q., Lin, C.Y., Liu, X.C., Elsworth, D., 2016. Types, characteristics and effects of natural fluid pressure fractures in shale: a case study of the paleogene strata in eastern China. Petroleum Explor. Dev. 43, 634–643.
Meng, Q.R., Kang, Z.Q., Zhao, Y.S., Yang, D., 2010. Experiment of thermal cracking and crack initiation mechanism of oil shale. Zhongguo Shiyou Daxue Xuebao 34, 89–92 (in Chinese with English abstract).
Mighani, S., Sondergeld, C.H., Rai, C.S., 2016. Observations of tensile fracturing of anisotropic rocks. SPE J. 21, 1289–1301.
Misra, S., Mandal, N., Dhar, R., Chakraborty, C., 2009. Mechanisms of deformation localization at the tips of shear fractures: findings from analogue experiments and field evidence. J. Geophys. Res. Solid Earth 114 (B4).
Ovid'Ko, I.A., 2007. Review on the fracture processes in nanocrystalline materials. J. Mater. Sci. 42, 1694–1708.
Ozkaya, I., 1984. Computer simulation of hydraulic fracturing in shales-influences on primary migration. J. Petroleum Technol. 36, 826–828.
Ozkaya, I., 1988. A simple analysis of oil-induced fracturing in sedimentary rocks. Mar. Petroleum Geol. 5, 293–297.
Panahi, H., Kobchenko, M., Renard, F., Mazzini, A., Scheibert, J., Dysthe, D.K., 2013. A 4D synchrotron X-ray tomography study of the formation of hydrocarbon migration pathways in heated organic-rich shale. SPE J. 18, 366–377.
Plank, R., Kuhn, G., 1999. Fatigue crack propagation under non-proportional mixed mode loading. Eng. Fract. Mech. 62, 203–229.
Potluri, N., Zhu, D., Hill, A. D., 2005. The effect of natural fractureson hydraulic fracture propagation. Paper SPE 94568 Presented at the SPE European Formation Damage Conference, Sheveningen, The Netherlands, 25–27 May.
Přikryl, R., 2001. Some microstructural aspects of strength variation in rocks. Int. J. Rock Mech. Min. Sci. 38, 671–682.
Rice, J.R., 1968. A path independent integral and the approximate analysis of strain concentration by notches and cracks. J. Appl. Mech. 35, 379–386.
Rodrigues, N., Cobbold, P.R., Loseth, H., Ruffet, G., 2009. Widespread bedding-parallel veins of fibrous calcite ('beef') in a mature source rock (Vaca Muerta Formation, Neuquén Basin, Argentina): evidence for overpressure and horizontal compression. J. Geol. Soc. 166, 695–709.
Sayers, C.M., 2013. The effect of anisotropy on the Young's moduli and Poisson's ratios of shales. Geophys. Prospect. 61, 416–426.
Schmidt, R.A., 1977. Fracture mechanics of oil shale-unconfined fracture toughness, stress corrosion cracking, and tension test results. In: Wang, F.-D., Clark, G.B. (Eds.), Energy Resources and Excavation Technology: Proceedings, 18th U.S. Symposium on Rock Mechanics. Colorado School of Mines, Golden, Colorado, 2A2-1–2A2-6.
Sondergeld, C.H., Rai, C.S., 2011. Elastic anisotropy of shales. Lead. Edge 30, 324–331.
Sone, H., Zoback, M.D., 2013a. Mechanical properties of shale-gas reservoir rocks-Part 1: static and dynamic elastic properties and anisotropy. Geophysics 78, D381–D392.
Sone, H., Zoback, M.D., 2013b. Mechanical properties of shale-gas reservoir rocks-Part 2: ductile creep, brittle strength, and their relation to the elastic modulus. Geophysics 78, D393–D402.
Vernik, L., 1994. Hydrocarbon-generation-induced microcracking of source rocks. Geophysics 59, 555–563.
Waters, G. A., Lewis, R. E., and Bentley, D. C. 2011. The effect of mechanical properties anisotropy in the generation of hydraulic fractures in organic shales. SPE 146776, Annual Technical Conference and Exhibition, Denver, Colorado, USA, 30 October-2 November.
Yassir, N.A., Bell, J.S., 1994. Relationships between pore pressure, stresses, and present-day geodynamics in the Scotian shelf, offshore eastern Canada. AAPG Bull. 78, 1863–1880.